Cenozoic evolution of the eastern Black Sea: a test of depth-dependent stretching models

Donna J. Shillington[1*], Nicky White[2], Timothy A. Minshull[1], Glyn R.H. Edwards[2], Stephen M. Jones[3], Rosemary A. Edwards[1], Caroline L. Scott[1]

[1]National Oceanography Centre, Southampton, Univ. Southampton, European Way, Southampton SO14 3ZH, UK

[*]corresponding author, djshill@noc.soton.ac.uk, phone +44 (0) 2380596614, fax +44 (0)2380593059

[2]Bullard Laboratories, Departments of Earth Sciences, Univ. Cambridge, Madingley Road, Cambridge CB3 0EZ, UK

[3]Trinity College, Department of Geology, Dublin 2, Ireland

resubmitted to *Earth Planet. Sci. Lett.*, October 2007

Abstract

Subsidence analysis of the eastern Black Sea basin suggests that the stratigraphy of this deep, extensional basin can be explained by a predominantly pure-shear stretching history. A strain-rate inversion method that assumes pure-shear extension obtains good fits between observed and predicted stratigraphy. A relatively pure-shear strain distribution is also obtained when a strain-rate inversion algorithm is applied that allows extension to vary with depth without assuming its existence or form. The timing of opening of the eastern Black Sea, which occupied a back-arc position during the closure of the Tethys Ocean, has also been a subject of intense debate; competing theories called for basin opening during the Jurassic, Cretaceous or Paleocene/Eocene. Our work suggests that extension likely continued into the early Cenozoic, in agreement with stratigraphic relationships onshore and with estimates for the timing of arc magmatism. Further basin deepening also appears to have occurred in the last ~20 m.y. This anomalous subsidence event is focused in the northern part of the basin and reaches its peak at ~15-10 Ma. We suggest that this comparatively localized shortening is associated with the northward movement of the Arabian plate. We also explore the effects of paleowater depth and elastic thickness on the results. These parameters are controversial, particularly for deep-water basins and margins, but their estimation is a necessary step in any analysis of the tectonic subsidence record stored in stratigraphy.

Keywords: Black Sea, extension, subsidence, strain rate

1. Introduction

To understand the temporal and spatial evolution of highly extended lithosphere, it is important to analyze regions with a complete record of subsidence and crustal thinning using theoretical models that do not make prior assumptions about the style, duration or magnitude of stretching. Many questions remain about the importance and form of depth-dependent stretching during rifting. Some models call for a lateral offset between the locus of extension in the crust and mantle lithosphere (Wernicke, 1985; Hopper and Buck, 1998) or an increase or decrease in the amount of stretching with depth (Davis and Kusznir, 2004). The most extreme examples of depth-dependent stretching are associated with lower crustal flow during the extension of hot lithosphere with a thick crust (McKenzie et al., 2000) or with denudation of the lower crust and/or lithospheric mantle during the extension of cold lithosphere (Whitmarsh et al., 2001; Lavier and Manatschal, 2006). Variations in stretching with depth can have a significant effect on the thermal and subsidence history of basins and margins (Buck et al., 1988) and thus are important for practical applications, such as modeling the maturation of hydrocarbons.

Despite the importance of understanding variations in stretching with depth through the lithosphere, characterizing these variations is often difficult because of a lack of observations. Sedimentary infill is a record of subsidence, which is sensitive to thinning throughout the lithosphere. However, many well-studied margins are sediment-starved, and the subsidence record is difficult to reconstruct in the absence of independent constraints on paleobathymetry. In order to gain a complete picture of extension throughout the lithosphere, we must examine a basin whose crustal structure can be accurately constrained (i.e., from wide-angle refraction data) and that contains a complete sedimentary record (Davis and Kusznir, 2004). The eastern Black Sea (EBS) is an extensional basin that is thought to have opened in the Upper Cretaceous/early

68 Cenozoic (Zonenshain and Le Pichon, 1986; Robinson et al., 1995b) and contains 8-10 km of
69 sediments that record the Cenozoic history of this basin. Results of previous seismic refraction
70 and gravity studies imply that significant degrees of extension were involved in the formation of
71 this basin ($\beta > 4$) (Letouzey et al., 1977; Belousov et al., 1988; Starostenko et al., 2004). These
72 characteristics, together with the availability of a new wide-angle seismic dataset (Minshull et
73 al., 2005), industry seismic reflection data, and well control (Robinson et al., 1995b), make the
74 EBS an ideal natural laboratory for studying extensional processes. Furthermore, the Black Sea
75 is a frontier basin for hydrocarbon exploration, making it a timely target for study (Robinson et
76 al., 1996).

77 For the last thirty years, extensional sedimentary basins and passive margins have been
78 modeled using a range of kinematic and dynamic models. Kinematic models are concerned with
79 the movement of material and heat without reference to force, rheology or mass. The simplest
80 kinematic models assume that rifting is instantaneous and that the lithosphere thins uniformly
81 (McKenzie, 1978). More realistic kinematic models allow for finite-duration rifting and non-
82 uniform thinning of the lithosphere in one or two dimensions. Dynamic models attempt to solve
83 the general problem of how body forces act upon lithospheric rheology to deform the lithosphere
84 and generate subsidence. Many sophisticated dynamic models exist, but they are predicated upon
85 our understanding of the rheology of the crust and lithosphere, which is still relatively poor. The
86 vast majority of kinematic and dynamic models solve the forward problem whereby crustal
87 deformation and subsidence are calculated from a prescribed lithospheric stretching history
88 rather than the inverse problem, whereby the spatial and temporal history of lithospheric
89 deformation is extracted from subsidence and crustal data. The inverse approach is advantageous
90 because it allows trade-off between the governing parameters to be investigated in a formal way,

and we adopt this approach here. Kinematic models are preferable for use within an inverse scheme because they are simpler and less computationally intensive than dynamic models.

To extract an extensional history of the EBS and to address generic questions about continental extension, we use a kinematic algorithm that does not make any assumptions regarding the timing, duration, location, or magnitude of extension (White and Bellingham, 2002). This method inverts the backstripped sedimentary record for spatial and temporal variations in strain rate assuming pure-shear extension. We also present the results of applying an extended version of this algorithm that allows for depth-dependent stretching without assuming its existence or style (Edwards, 2006; Edwards et al., in prep). Although the EBS has been the subject of subsidence analysis and other modeling in previous studies (Robinson et al., 1995a; Spandini et al., 1996; Meredith and Egan, 2002; Cloetingh et al., 2003; Nikishin et al., 2003), the work presented here makes the fewest assumptions about the extensional history. We also explore the consequences of changing the most controversial variables required for subsidence analysis of deep basins and margins: paleowater depth and elastic thicknesses, T_e.

2. Geology of the Black Sea

The Black Sea region has experienced several episodes of extension and shortening since the Permian (Yilmaz et al., 1997; Robertson et al., 2004), and it continues to experience deformation today in response to the northward movement of the Arabian plate and westward escape of the Anatolian block along the North and East Anatolian Faults (McKenzie, 1972; McClusky et al., 2000). The basin is generally considered to have formed in a back-arc extensional environment because of its close spatial association with the subduction of both the Paleo- and Neo-Tethys Oceans, but the timing and style of this opening history remain controversial (Zonenshain and Le Pichon, 1986; Okay et al., 1994; Banks et al., 1997). The

114 Black Sea can be subdivided into eastern and western basins based on its basement structures;
115 these sub-basins are separated by the Archangelsky and Andrusov Ridges, which constitute a
116 system of buried basement ridges that run SW-NE through the center of the Black Sea and are
117 collectively called the Mid Black Sea High (Fig. 1). Based on plate reconstructions and the ages
118 of volcanic rocks with arc signatures located in the western Pontides, in northern Turkey (Görür,
119 1988; Okay et al., 1994), a Middle to Upper Cretaceous opening is estimated for the western
120 Black Sea (WBS). Analysis of seismic refraction and gravity datasets give a crustal thickness of
121 7-8 km and velocities consistent with a "basaltic" composition in the basin center, suggesting
122 that rifting in the WBS culminated in seafloor spreading (Letouzey et al., 1977; Belousov et al.,
123 1988; Starostenko et al., 2004).
124 Much less agreement exists on the timing of opening in the EBS. Alternative theories call
125 for a primary phase of opening in the Jurassic, Cretaceous (Zonenshain and Le Pichon, 1986;
126 Okay et al., 1994; Nikishin et al., 2003), Early Eocene/Paleocene (Robinson et al., 1995b; Banks
127 et al., 1997), or Eocene (Kazmin et al., 2000; Vincent et al., 2005). The age of the EBS infill is
128 estimated to be Cenozoic (Finetti et al., 1988); this observation together with documented
129 structural relationships at the edges of the basin, ages of arc magmatic products, and plate
130 reconstructions indicate that major basin-forming events probably occurred in the late Mesozoic
131 or early Cenozoic (Zonenshain and Le Pichon, 1986; Okay et al., 1994; Banks et al., 1997;
132 Boztug et al., 2004). Apatite fission track data suggest that arc magmatism in the Central
133 Eastern Pontides lasted until the mid-Paleocene and was followed by uplift related to the onset of
134 continental collision in the Late Paleocene to Early Eocene (Boztug et al., 2004), implying that
135 back-arc extension in the EBS occurred between the Upper Cretaceous and early Cenozoic.
136 Stratal relationships on the Shatsky Ridge where it is exposed onshore in Georgia also indicate

an Upper Cretaceous/Paleocene-Eocene timing for opening. In this location, sediments as young as Danian (earliest Paleocene) are unconformably overlain by mudstones of Upper Eocene age (Banks et al., 1997). Likewise, Eocene mudstones overlie Cretaceous chalks and volcanic rocks on Shatsky Ridge (Rudat and Macgregor, 1993). Carbonate rocks of Upper Cretaceous age were drilled at Chaladidi-13, Chaladidi-14, Ochamchira and Akcakoca (Fig. 1), whereas the early Cenozoic section is typically comprised of mudrocks, implying that basin deepening occurred in this time interval.

Most reconstructions show the EBS opening in a NE-SW direction by the rotation of the Shatsky Ridge away from the Mid Black Sea High (Okay et al., 1994; Nikishin et al., 2003) (Figs. 1 and 2). It is uncertain whether opening of the EBS concluded with initial seafloor spreading; previous gravity and seismic studies have estimated a crustal thickness of ~10-11 km in the basin center and seismic velocities lower than average oceanic crust, implying a thinned continental origin (Belousov et al., 1988; Starostenko et al., 2004), although this interpretation is disputed (Letouzey et al., 1977; Zonenshain and Le Pichon, 1986). Preliminary results from the new wide-angle dataset indicate a crustal thickness as small as 7 km and velocities consistent with thinned continental crust or oceanic crust produced in a back-arc setting (Minshull et al., 2005). Further work is needed to ascertain the nature of this crust. For the purposes of this paper, we will assume that crust in the center of the EBS is stretched continental crust. We discuss the implications of our results if crust in the center of the EBS is oceanic in Section 8.3.

3. Database: Seismic Reflection and Well-log Data

Several seismic and lithological datasets are available in the EBS that can be used to derive inputs for subsidence analysis. Academic and industry seismic reflection profiles have previously been acquired throughout the EBS. We have chosen to model the subsidence history

along a transect where coincident wide-angle data have recently been collected (Fig. 1). It lies orthogonal to the thinnest crust in the basin as delineated by gravity data and is roughly parallel to the inferred opening direction (Starostenko et al., 2004). This line also encompasses major extensional features in the EBS. It begins near Samsun, crosses Sinop Trough, Archangelsky Ridge, the basin center, Shatsky Ridge, Tuapse Trough and terminates at the Russian margin west of Tuapse (Figs. 1 and 2).

Many significant characteristics of the EBS basin can be observed in the seismic reflection profiles (KDZ 91-43 and Line 8040) along this line (Fig. 2). Sediments in the center of the basin are remarkably undeformed, suggesting that shortening due to the northward movement of the Arabian plate is limited to the eastern edge of the Black Sea (Rangin et al., 2002) and to the Greater Caucaus (McClusky et al., 2000; Saintot and Angelier, 2002). Within the sedimentary section, several units can be identified, including the Maikop Formation, a clay-rich unit that constitutes the major potential hydrocarbon source rock in the Black Sea (Robinson et al., 1996). The Top-of-Cretaceous horizon can also be identified, which is interpreted to represent the contact between Eocene and Paleocene mudstones and Upper Cretaceous carbonate and volcanogenic sedimentary rocks (Zonenshain and Le Pichon, 1986; Robinson et al., 1996). To the north of the basin center lies the Shatsky Ridge, a basement high bound to the south by one or more large normal faults (Banks et al., 1997), but whose northern side is being flexed beneath the Greater Caucaus, generating a small foreland basin, the Tuapse Trough (Fig. 2). The Archangelsky Ridge has very steep sides, but few extensional structures can be discerned within the crust. Farther south lies the Sinop Trough, which is also interpreted to be extensional in origin; this sub-basin deepens to the west and ultimately connects to the WBS.

Information on the age and lithology of the stratigraphic units in the Black Sea region comes from drilling and onshore geologic mapping (Fig. 1, Appendix). Sediments as old as Late Miocene have been sampled in the center of the Black Sea by three DSDP sites (Fig. 1) (Ross et al., 1978), and sediments as old as Late Jurassic have been recovered by industry wells at the margins of the Black Sea (e.g., Ochamchira and Akcakoca; Fig. 1) (Zonenshain and Le Pichon, 1986; Banks et al., 1997). The lithology and age of these units are used in subsidence analysis and provide critical information on the opening history of the EBS (see the Appendix for brief review).

4. Deriving inputs for subsidence analysis

For subsidence analysis, we require a series of layers with assigned ages, lithologies and paleowater depth histories and a template for the initial configuration of the crust and mantle lithosphere. Each of these inputs is described below.

4.1 Stratigraphic framework

In order to estimate the ages and lithologies of sedimentary units in the eastern Black Sea, seismic stratigraphic horizons have been tied to well control at the edges of the basin using 2D and 3D industry seismic datasets (Figs. 2 and 3) (Robinson et al., 1996). The geologic time scale of Gradstein et al. (2004) is used. Links between chronostratigraphy and regional stratigraphy are taken from Jones and Simmons (1997). There are several difficulties in developing a stratigraphic framework for the EBS. First, all of the wells that penetrate the entire Cenozoic section and part of the Mesozoic section are necessarily located on the margins of the Black Sea or onshore, while strata of this age lie at depths >8 km in the center of the basin (Fig. 1). Thus, stratigraphic sections at well locations are comparatively condensed, and some uncertainties are associated with tracing major horizons from well locations into the basin center. Furthermore,

most offshore well control lies in the WBS (e.g., Akcakoca, Fig. 1). Tracing horizons from the western basin to the eastern basin is complicated by the presence of the Mid Black Sea High, which prevents direct correlation of horizons older than Late Eocene (Banks et al., 1997). However, correlations presented here use all available well control and seismic reflection data in the region and are consistent with other recent interpretations (Robinson et al., 1995a; Spandini et al., 1996; Meredith and Egan, 2002), and thus are the best available estimates of the ages and lithologies of the infill of the EBS.

A second important issue in using seismic reflection data to constrain stratigraphy is conversion between two-way travel time and depth (Fig. 2). We used interval velocities derived from stacking velocities provided by BP for depth conversion (Fig. 2). Because most of the seismic reflection data located in the Black Sea were acquired with either a 4- or 6-km-long streamer, these data cannot constrain the velocities of deeper strata (~>4-6 km). The inset in Figure 2a shows the average depth-time relationship for sediments with upper and lower bounds based on +/- one standard deviation in velocity, calculated by comparing velocity functions over a 150-km-long segment within the center of the EBS. Part of the variation in velocity structure included in this envelope could be caused by real changes in sediment properties and basin structure. However, it provides an illustration of approximate uncertainties. The standard deviation in velocity increases steadily with depth from ~60 m/s at 3 s to ~140 m/s at 5.5 s. Below this depth, the standard deviation increases more rapidly to 345 m/s at 8.75 s, at the Top-of-Cretaceous horizon (Fig. 2b); this increase is associated with depths at which velocities would be less well constrained due to short streamer length. These uncertainties in velocity are associated with uncertainties in depth of ~20 m at 3 s, ~275 m at 5.5 s, and ~1000 m at 8.75 s. A comparison between stacking velocities used by BP and velocities derived by preliminary

228 modeling of wide-angle seismic data (Minshull et al., 2005), which have a sufficiently large
229 aperture to constrain the velocities of deep sediments, shows that the two velocity functions are
230 very similar.

231 **4.2 Paleowater depth**

232 The paleowater depth (PWD) of each horizon is required for backstripping, but PWD
233 histories are notoriously difficult to constrain for deep-water basins and continental margins.
234 Consequently, as for any subsidence study of a deep-water basin or margin, PWD constitutes a
235 significant source of uncertainty in our analysis of this region. Variations in water depth of at
236 least ~2200 m are possible based on the current bathymetry of the Black Sea, and some authors
237 estimate even more dramatic variations (Robinson et al., 1995a; Spandini et al., 1997). Previous
238 subsidence models have assumed or inferred a large range of PWD histories: (1) Robinson et al.
239 (1995a) and Cloetingh et al. (2003) use the results of the forward model of Spandini et al. (1996)
240 to infer PWD variations as great as ~4500 m through the Cenozoic; (2) Nikishin et al. (2003)
241 propose shallow PWD in the mid-Cretaceous and deep PWD thereafter; (3) Meredith and Egan
242 (2002) assume that all of the accommodation space was filled with sediment throughout the
243 history of the basin in the 2D portion of their analysis (Fig. 3). In reality, very few constraints
244 exist on the PWD of different intervals in the Black Sea except those than can be inferred from
245 interpreted lithologies within the basin and stratigraphic relationships (e.g., Shatsky Ridge).

246 Here, we consider three end-member PWD cases (Fig. 3): (1) The EBS was shallow at
247 the end of the Cretaceous/beginning of the Cenozoic (0-200 m), after which it was deep (2000-
248 2200 m) until the present; (2) The EBS was deep (2000-2200 m) at the end of the Cretaceous and
249 remained so until the present; (3) The EBS was shallow (0-200 m) until the end of the Pliocene
250 and deep (2000-2200 m) afterwards. For each of these cases, the depth of the seabed at 0 Ma is

set to the current bathymetry in the EBS, where the maximum depth is ~2200 m. These histories are relatively simple yet encompass the key characteristics of paleowater depth histories employed in previous studies (Fig. 3).

4.3 Crustal and lithospheric template

In addition to information on the depth, age, lithology, and paleowater depth of sedimentary horizons, the crustal and lithospheric template must be defined (White and Bellingham, 2002). Crustal thickness increases south of the Black Sea from 35 km near the edge (Çakir and Erduran, 2004) to 46 km in the eastern Anatolian plateau (Zor et al., 2003). These crustal thicknesses are likely affected by recent shortening due to the northward movement of the Arabian plate. We therefore have set the initial crustal thickness to 32 km, consistent with preliminary results from modeling of wide-angle seismic data near the SW edge of the basin (Minshull et al., 2005).

Initial lithospheric thickness and temperature structure are more difficult to determine. Constraints on the present-day temperature of the lithosphere beneath the Black Sea region come primarily from measurements of seismic velocity and attenuation. The results of *p*-wave tomography and *s*-wave attenuation studies indicate that the mantle beneath the eastern Black Sea has higher velocities and is associated with less attenuation than the surrounding regions (e.g., Anatolia), suggesting comparatively cold mantle temperatures (Hearn and Ni, 1994; Gök et al., 2003; Al-Lazki et al., 2004). Heat flow values within the basin are complicated by the thick sedimentary infill, and thus are difficult to interpret (Kutas et al., 1998). Although these lines of evidence provide constraints on mantle temperatures at present, they may not accurately reflect thermal conditions at the time of rifting. Seismic reflection profiles do not show evidence for seaward dipping reflections or other indications of abundant synrift magmatism nor is there any

evidence for flood basalt volcanism onshore, so we infer that mantle temperatures were not unusually high at this time. Consequently, we assume a 'normal' temperature for the base of the lithosphere of 1333ºC, which is consistent with a potential temperature of 1300ºC for the upper mantle (Bellingham and White, 2002).

Even less information is available regarding lithospheric thickness. White and Bellingham (White and Bellingham, 2002) demonstrated that the ratio of crustal to lithospheric thickness is more important in controlling the outcome of subsidence analysis than the absolute value assigned to either parameter. Assuming that the top of the crust is at sea level, they balanced a section of continental lithosphere with a standard mid-ocean ridge to demonstrate that a ratio of crustal to lithospheric thickness of ~1:3.6 is in isostatic equilibrium (White and Bellingham, 2002). In the case of the EBS, this assumption is justified because lithological data suggest that Upper Cretaceous sediments were deposited in a shallow water environment (Appendix). For our initial crustal thickness of 32 km and an average crustal density of 2.78 g/cm^3, this ratio prescribes a lithospheric thickness of ~120 km, which we use for this study.

4.4 Elastic Thickness, T_e

The flexural rigidity of the lithosphere, often expressed as elastic thickness (T_e), dictates how the lithosphere responds to a load. If the lithosphere is strong, a load is compensated over a large area, and if the lithosphere is weak, a load is compensated locally. Although T_e may be a fundamental characteristic modulating the response of the lithosphere to a range of loading phenomena, its estimation is controversial, even in the oceanic domain (Burov and Diament, 1995; McKenzie and Fairhead, 1997; Perez-Gussinye et al., 2004; Bry and White, 2007). Here, we backstrip and model subsidence using a range of values for T_e (0 to 100 km) and discuss the consequences of varying T_e for the results and data fit in Section 8.2.

5. Data Preparation

The parameters shown in Figure 3 and described in Section 4 are used to flexurally backstrip each sedimentary layer using the method of Steckler and Watts (1978) and Sclater and Christie (1980), modified after Jones et al. (2004). The backstripping method applied here allows for variable PWD across the basin, which is important for correctly modeling the edges of the basin. We scale present-day bathymetry along each transect to create a series of profiles of PWD across the basin for each horizon. Following backstripping, a filter is applied to each horizon to remove small-scale structures that might be associated with individual faults so that regional tectonic subsidence can be isolated for strain rate inversion (Bellingham and White, 2002; Jones et al., 2004). We filtered our horizons using a cosine filter with a length of 40 km, although using different filter lengths (e.g., 20 km), or not using a filter at all, does not alter the results of inversion (Jones et al., 2004).

Previous studies indicate that the differences in water-loaded stratigraphy arising from changing the lithology used for backstripping are sufficiently minor that they do not significantly change the results of strain rate inversion (Bellingham and White, 2002). Paleowater depth and elastic thickness, however, have much larger impacts on the amount of tectonic subsidence implied after backstripping (see online supplementary material). Below, we apply both depth-uniform and depth-dependent strain rate inversions to all three PWD cases for a range of values of T_e (0-100 km).

6. Strain Rate Inversion

We used the backstripped stratigraphy and parameters described above as input into strain rate inversion (White and Bellingham, 2002; Jones et al., 2004). For a complete description of other variables assigned for modeling, see White and Bellingham (2002). This

method uses water-loaded stratigraphic horizons to invert for spatial and temporal variations in strain rate using a kinematic approach. Strain rate is considered to be the fundamental parameter describing extension, and it can be used to calculate stretching factors, β (White, 1993). We first apply an algorithm that assumes depth-uniform stretching (White and Bellingham, 2002; Jones et al., 2004). We then apply a new version of this algorithm that allows stretching to vary with depth, but does not presuppose either the existence or style of depth dependence (Edwards, 2006; Edwards et al., in prep).

The forward model of both algorithms, which relates strain rate to subsidence, involves four steps (White, 1993; White and Bellingham, 2002). First, a given distribution of strain rate in space and time dictates a velocity field for the deformation of the lithosphere. Secondly, lithospheric thinning perturbs the thermal structure by bringing warmer asthenosphere to shallower levels. The thermal evolution of the lithosphere is solved using the 2D heat flow equation, including horizontal and vertical advective terms. Thirdly, if a linear relationship is assumed between temperature and density, the calculated temperature structure of the lithosphere can be used to determine temporal and spatial variations in density. Lateral and vertical density variations impose loads on the lithosphere. Lastly, these loads result in subsidence or uplift; the magnitude and shape of this subsidence is moderated by T_e.

The relationship between subsidence and strain rate outlined above for the forward model can be used to solve the inverse problem, in which the strain rate field is determined from known stratigraphy. A strain-rate history is found by minimizing the difference between observed and predicted stratigraphy. To regularize the inversion, first and second derivative smoothing in time and space and positivity weighting functions are also included in the misfit function (White and Bellingham, 2002). In the depth-uniform algorithm, strain rate is also fixed to be constant with

343 depth, and the global minimum of the misfit function is found using a conjugate gradient method
344 that performs successive line minimizations (Powell's algorithm) (Press et al., 1992).
345 Additional considerations are needed in allowing for variations in extension with depth
346 during inversion. First, mass must be conserved (i.e., the cumulative strain across the model must
347 be identical at all depths). Mass conservation is easily achieved if strain rate does not vary with
348 depth; to ensure that this requirement is still met in the depth-dependent algorithm, we use depth-
349 dependent strain-rate distributions based on periodic functions (e.g., Fourier series) horizontally
350 and linear splines with depth (Edwards, 2006; Edwards et al., in prep). During inversion, we
351 invert for the coefficients of these periodic functions, which allows us to retrieve the depth
352 dependency of strain rate whilst automatically conserving mass and honoring the boundary
353 conditions. Secondly, the inversion routine is weighted to favor depth-independent strain rate
354 solutions, so that depth-dependent stretching is only invoked when pure-shear stretching cannot
355 explain the observations. Finally, when depth-dependent stretching is required to fit the data, the
356 form of depth dependency is not prescribed. The details of the depth-dependent algorithm are
357 described by Edwards (2006).

358 **7. Results**

359 The results of inverting this line assuming Airy isostasy (i.e., $T_e = 0$ km) using both
360 depth-uniform and depth-dependent algorithms for the three PWD cases described in Section 4.2
361 are presented in Figures 4-6 and discussed in Sections 7.1-7.3; key strain rates and errors are
362 given in Table 1. The effects of backstripping and inverting for stratigraphy with other values of
363 T_e are illustrated in Figure 7 and discussed in Section 7.4.

7.1. Case 1: Shallow at the end of the Cretaceous and deep afterwards

Two primary strain rate events can be identified following inversion. The first event continues from the end of the Cretaceous (the age of the oldest horizon included in inversion) until the Middle Eocene (~65-45 Ma; Fig. 4, Table 1). A period of quiescence follows until the Middle Miocene (~15-10 Ma), when a second, smaller subsidence anomaly is evident. This event is observed across the profile but is most pronounced in the northeastern parts of the profiles. The match between observed and predicted tectonic stratigraphy is excellent (Fig. 4, Table 1). This strain rate history predicts a maximum cumulative β (from 65 Ma to present) of ~4.8, which is similar to the β calculated based on initial velocity modeling of coincident wide-angle data (Minshull et al., 2005) (Fig. 4).

The depth-dependent inversion yields a very similar temporal strain rate distribution to the depth-uniform inversion. The fits between observed and predicted horizons are also good (Table 1). A significant result of the depth-dependent inversion is the relatively simple distribution of strain rates in depth. The depth slice at 58.5 Ma in Figure 4 shows that the strain rate event broadens with depth beneath the center of the basin, but is otherwise symmetric. The most convincing depth dependence observed in this model is associated with Sinop Trough, on the southern side of the basin. Here, an increase in strain rate with depth is apparent, and this event appears to coalesce with the strain rate event associated with the basin center.

7.2 Case 2: Deep from the end of the Cretaceous to the present

Although some strain rate events are required in the Cenozoic even if the basin has been deep since the end of the Cretaceous (Fig. 5, Table 1), these are not as great in magnitude as the primary strain rate event found for Case 1. A small strain rate event can be observed at 65 Ma, which widens and reaches its peak value in the Late Eocene. A second anomaly around 15-10

Ma that is focused in the northern part of the basin is also evident in the results from Case 2, similar to the one observed in Case 1; the 15-10 Ma events for both Cases 1 and 2 are also of similar magnitude. The results of inversion for this PWD case also yield a very good fit between observed and predicted backstripped stratigraphy (Table 1).

A much smaller cumulative β (~2) is indicated by the strain rate distribution for Case 2 (Fig. 5). This result suggests that even if the EBS already contained 2000-2200 m of water by the end of the Cretaceous, additional tectonic subsidence is required to explain the present-day basin. The discrepancy between the β value of Case 2 and the one calculated from the results of initial modeling of wide-angle seismic data (Fig. 5) might be explained by significant extension before the Cenozoic that would not be recovered by the sediment record employed in this study, which begins at 65 Ma.

A similar strain rate distribution is recovered by depth-dependent inversion. As in Case 1, almost no depth dependency is associated with the strain rate distribution at the end of Cretaceous times except a slight broadening towards the base of the lithosphere.

7.3 Case 3: Shallow until the end of the Pliocene and deep afterwards

Inversion of horizons backstripped using the third PWD case yields the worst fits between observed and predicted horizons (Fig. 6, Table 1). One primary strain rate event is recovered from 20-0 Ma, and the cumulative β is ~14 (Fig. 6). Other short-wavelength strain rate peaks are also recovered at earlier times. The depth-dependent inversion is more successful in matching observed and predicted backstripped horizons, but still has the highest associated misfit of all of the PWD cases. Again, the significant strain rate event occurs between 20-0 Ma, and short-wavelength fluctuations in strain rate can be observed in time and space.

7.4 Effect of T_e on results

410 The results discussed above (Figs. 4-6) assume Airy isostasy (i.e., $T_e = 0$ km). To explore
411 the consequences of non-zero T_e, we have also backstripped and inverted stratigraphy for PWD
412 Cases 1 and 2 with larger values for T_e (20, 50, and 100 km); PWD Case 3 was excluded due to
413 the poor data fits following inversion even for Airy isostasy. When larger values of T_e are used to
414 backstrip and model stratigraphy, the primary effect is that higher strain rates and larger
415 stretching factors are recovered by inversion (Fig. 7). One of the primary reasons for this result
416 is that the tectonic subsidence recovered by backstripping a stratigraphic section using a large T_e
417 is greater than that recovered by backstripping the same section using small T_e because the
418 lithosphere is less sensitive to loading (or unloading) when T_e is higher (see online
419 supplementary material). For example, a maximum of ~5 km of tectonic subsidence is suggested
420 for PWD Case 1 when T_e is 0 km, and ~6.1 km when T_e is 50 km. As a result, the strain rates and
421 stretching factors recovered by inverting tectonic subsidence for high values of T_e are
422 correspondingly large. A maximum stretching factor of ~4.8 is recovered by inversion for PWD
423 Case 1 when T_e is 0 km, and ~7.4 when T_e is 50 km.
424 Although the inferred magnitude of extension increases for increasing values of T_e, the
425 temporal and spatial patterns recovered using different values of T_e are similar (Fig. 7). The
426 strain rate distributions for larger values of T_e are slightly more focused in the center of the basin
427 than those for the Airy isostasy case, reflecting the sharper basin geometries after backstripping
428 using large T_e (Fig. 7). The fit between observed and predicted horizons worsens with increasing
429 T_e, particularly for values between 0 and 20 km.

8. Discussion

8.1. Choosing between PWD cases

Strain rate inversion of the three PWD cases described above shows that Cases 1 and 2 produce acceptable data fits (Table 1) and plausible strain rate distributions. The inability of either inversion algorithm to match observed and predicted tectonic subsidence for Case 3 indicates that the PWD assumptions in this case are unrealistic. Lack of independent evidence for Miocene or Pliocene extension casts further doubt over the validity of Case 3. Although inversions for both Cases 1 and 2 fit the data equally well, we prefer Case 1 for the following reasons. First, the assumptions in Case 1 about PWD variations through time are more consistent with what is known about lithology and geology of each of the intervals from the edges of the basin. Secondly, Case 1 is supported by limited examples of growth in seismic reflection sections from the EBS (Fig. 8).

Where Upper Cretaceous sections have been described from drilling or onshore mapping, they are primarily composed of carbonate and/or volcanogenic sedimentary rocks, whereas the Paleocene/Eocene interval comprises pelagic mudrocks (Robinson et al., 1996). Furthermore, Eocene mudstones have been observed to unconformably overly Paleocene and Cretaceous units on Shatsky Ridge where it has been drilled and studied in outcrop onshore (Banks et al., 1997) and Cretaceous chalks, tuffs and volcanic rocks where they were dredged on Archangelsky Ridge (Rudat and Macgregor, 1993). These stratal relationships and changes in lithology are most easily interpreted as representing an increase in PWD. This analysis shows that an extensional strain rate event that predicts values for β similar to those calculated from initial results of modeling wide-angle seismic data can explain a reasonable change in PWD at this level.

453 An obvious difficulty in dating the timing of extension within the EBS is the near-
454 absence of easily interpretable evidence of extension within any stratigraphic unit, such as
455 growth related to fault movement. However, limited evidence is available that corroborates the
456 results of Case 1 discussed above. For example, possible synrift fanning of early Cenozoic
457 sediments can be observed in Sinop trough (Fig. 8a) (Rangin et al., 2002). Additionally, possible
458 evidence of growth is occasionally observed in the basin, both adjacent to the Turkish margin
459 and in the center (Fig. 8b). If basin opening occurred quickly, as suggested by onshore evidence
460 (Ustaömer and Robertson, 1997), classic sedimentary features such as growth might not be easily
461 identified.
462 Although we favor Case 1, our analysis does not allow us to eliminate Case 2. The
463 results of Case 2 show that even if the EBS was already 2000-2200 m deep at the end of the
464 Cretaceous, additional tectonic subsidence is still required in the early Cenozoic to explain the
465 stratigraphic architecture.
466 **8.2 What is the elastic thickness?**
467 As discussed in Section 7.4, the primary effect of using larger values of T_e to backstrip
468 and model the profiles is that greater amounts of tectonic subsidence are implied, and
469 correspondingly larger strain rates and stretching factors are recovered by inversion. The results
470 can be judged in terms of both misfit between data and predictions following inversion and
471 implied stretching factors. Smaller data misfits are associated with smaller values of T_e (< 20 km)
472 (Fig. 7). The misfit function flattens for T_e values greater than 20 km because the associated
473 flexural wavelengths are similar to or larger than the spatial dimensions of the eastern Black Sea
474 itself. For PWD Case 1, the results for T_e values of 50 km or higher also have very high
475 maximum stretching factors (>7) since stretching factors of 5.5-6 are commonly likened to

476 seafloor spreading. They also predict a crustal thickness of only ~4 km at the center of the basin,
477 which is smaller than the value indicated by wide-angle seismic data. For PWD Case 2, the
478 stretching factors recovered for all values of T_e are reasonable. These observations lead us to
479 favor the interpretation that the eastern Black Sea was relatively weak ($T_e \leq 20$ km) during much
480 of the Cenozoic. This result is consistent with an estimate of 2.3 km for T_e obtained by matching
481 the curvature of the Shatsky Ridge where it is flexed beneath the Caucaus with predicted curves
482 for a point-loaded, broken elastic beam (Fig. 7d) (Turcotte and Schubert, 2002).

483 **8.3 Implications of crustal type in the basin center for modeling results**

484 The analysis presented above assumes that the EBS is floored by thinned continental
485 crust. However, the nature of crust in the basin center is unknown, although initial results from a
486 recently acquired wide-angle seismic dataset in the EBS yield crustal velocities and thicknesses
487 along this line that could be compatible with either thinned continental crust or oceanic crust
488 produced in a back-arc setting (Minshull et al., 2005). Therefore, we must consider the
489 consequences for our results if the EBS is floored by oceanic crust. The results from Case 2 most
490 closely approximate the consequences of having oceanic crust in the center of the EBS. The
491 total amount of water-loaded subsidence observed in this model (~3250 m) is similar to the
492 amount that would be anticipated for 65-m.y.-old oceanic crust (Parsons and Sclater, 1977).
493 However, the EBS subsidence curve is not exponential like the depth-age relationship of Parsons
494 & Sclater (1977), implying that not all of this subsidence can be accounted for by cooling and
495 sinking of oceanic lithosphere even if the EBS is floored by oceanic crust.

496 **8.4 Evidence for regional shortening in last 20 m.y.**

497 A second subsidence anomaly is evident in the results of both the depth-dependent and
498 depth-uniform strain rate inversion for Cases 1 and 2, which reaches its peak around ~15-10 Ma,

but continues until 0 Ma (Figs. 4 and 5). This inversion algorithm interprets all such subsidence events as resulting from extensional strain. Although small subsidence anomalies are observed across the entire profile, it is primarily concentrated in the northeastern part of the basin. We propose that this event corresponds to subsidence resulting from shortening concentrated at the northern margin resulting from northward movement of the Arabian plate. This event is manifested in the flexure of the Shatsky Ridge beneath the Greater Caucaus (Fig. 2), but is also supported by the ages of syn-orogenic magmatism, reconstructions and paleostress indicators (Yilmaz et al., 1997; Saintot and Angelier, 2002; Nikishin et al., 2003). This observation is also consistent with GPS measurements of present-day deformation in the region, which show that some shortening is accommodated in the Caucaus, but that there is little evidence for internal deformation within the Black Sea itself (Reilinger et al., 2006). Cloetingh et al. (2003) and Nikishin et al. (2003) have also attributed basin-wide tectonic deepening of the EBS in the late Cenozoic to shortening.

8.5 Depth-uniform and depth-dependent stretching

One of the most important results of this study is the ability of a largely depth-uniform stretching model to account for the observed stratigraphy in the EBS. Even when extension is allowed to vary with depth, a relatively depth-uniform stretching history is recovered by inversion for both Cases 1 and 2 (Figs. 4 and 5). A slight broadening of the strain rate distribution with depth is recovered in the center of the basin, while a more pronounced increase in strain rate with depth is associated with Sinop Trough. However, these variations in stretching with depth are mild in comparison with those inferred for other basins (Edwards, 2006; Edwards et al., in prep). Furthermore, depth-uniform and depth-dependent inversions produce similarly good matches between predicted and observed horizons (Table 1). Therefore, we consider the

central basin of the eastern Black Sea to have formed predominantly by depth-uniform stretching. This study is the first time to our knowledge that a modeling algorithm that allows for any style of depth-dependent stretching has been applied to produce a relatively depth-uniform result.

8.6 Along-strike variations in extension in the EBS

To investigate possible changes in the amount of extension along strike in the EBS, we estimate β throughout the EBS using a relationship between β and sediment thickness derived from strain rate inversion results for PWD Case 1 (see inset in Fig. 9). This map was then filtered at 40 km to highlight regional trends and remove small-scale variations from individual faults. The result implies a first-order increase in extension to the east, which is illustrated by the increasing size of regions with $\beta > 5$ in this direction (Fig. 9). This overall trend is interrupted by intervening regions with lower apparent β values; these most likely arise from a series of NE-SW trending faults that offset the basement in the eastern basin (Finetti et al., 1988). This apparent eastward increase in the amount of extension is consistent with the idea that the EBS opened by rotation of the Shatsky Ridge away from the Mid Black Sea High (Fig. 1) (Okay et al., 1994), where the increasing distance between the Shatsky Ridge and Mid Black Sea High should be accompanied by increased β values.

9. Conclusions and Implications

The analysis presented here yields the following major results: 1) very little depth-dependence is required to explain the observed stratigraphy in the EBS, and a largely depth-uniform model is recovered by inversion even when depth-dependent stretching is permitted; 2) extension in the EBS most likely continued into the early Cenozoic, consistent with stratigraphic relationships and observations from onshore mapping; 3) subsidence analysis also identifies a

later subsidence anomaly (15-10 Ma) that is most pronounced in the northeastern part of the basin, which is likely related to shortening from northward movement of Arabian plate.

Acknowledgements

This work was supported by the Natural Environment Research Council (UK) (NER/T/S/2003/00114 and NER/T/S/2003/00885), BP and the Turkish Petroleum Company (TPAO). BP and TPAO generously provided access to the seismic reflection and well-log data that underpin this study. We would particularly like to thank G. Coskun (TPAO), A. Demirer (TPAO), A.J. Haines (Cambridge), R. O'Connor (BP), B. Peterson (BP), A. Price (BP), and K. Raven (BP) for their help. We would also like to thank A.H.F. Robertson for useful discussions. Constructive suggestions and reviews by S. Cloetingh, R. van der Hilst and an anonymous reviewer substantially improved the manuscript. University of Cambridge Department of Earth Sciences Contribution Number ES 8977.

Appendix: Stratigraphy

Upper Jurassic –Upper Cretaceous

Drilling at the margins of the Black Sea and mapping of time-correlative units onshore (e.g., Kapanbogazi and Inalti Fms) indicates that Upper Jurassic through Upper Cretaceous sedimentary rocks are comprised of a variety of lithologies, notably including shallow water carbonate rocks. Sections from this time period also contain significant volcanic material (Robinson et al., 1995a; Görür and Tüysüz, 1997). Carbonate rocks and chalks of this age have been drilled at Chaladidi-13, Chaladidi-14, Ochamchira and Akcakoca (Fig. 1) (Robinson et al., 1996; Banks et al., 1997). The Upper Cretaceous section exposed onshore south of Sinop is comprised of reefal limestone (Boyabat Limestone) and calciturbidites and limestones (Akveren Fm.) (Görür and Tüysüz, 1997).

Early Paleocene – Middle Eocene (45-65 Ma)

Time-correlative formations exposed in the western and eastern Pontides (Atbasi and Kusuri Fms.) are dominantly siliclastic turbidites, shallow and/or deep water mudstones, pelagic limestones and marls, often containing significant amounts of volcanogenic sediments (Robinson et al., 1995b; Görür and Tüysüz, 1997; Yilmaz et al., 1997). Similar lithologies were encountered by drilling onshore in Georgia (Chaladidi-13 and Chaladidi-14) (Banks et al., 1997). The characteristics of this interval in seismic sections implies that they were deposited as pelagic muds (Robinson et al., 1995a). However, information on this interval of EBS stratigraphy is limited due to its scant exposure onshore and in wells (Robinson et al., 1995b).

Middle Eocene – Top of Eocene (45-33.9 Ma)

Eocene formations exposed in the Pontides (Kusuri and Ayancik Fms.) are dominantly siliclastic turbidites (sandstones and shales) (Görür and Tüysüz, 1997; Yilmaz et al., 1997), and

583 siliclastic turbidites and limestones were drilled onshore in Georgia (Chaladidi-13 and Chaladidi-
584 14) (Banks et al., 1997). Carbonate, terrigenous deposits were also encountered in this interval
585 offshore Bulgaria (Zonenshain and Le Pichon, 1986).

586 ***Maikop Formation: Top of Eocene – Early Miocene (33.9-20.5 Ma)***

587 This stratigraphic unit comprises the most significant hydrocarbon source rock in the
588 Black Sea and Caspian regions. The deposition of muds rich in organic carbon is attributed to
589 anoxic conditions, and very little sand is observed in the Maikop Formation where it has been
590 sampled offshore (Robinson et al., 1996). Furthermore, the seismic transparency observed
591 within this unit in seismic reflection profiles suggests a homogeneity in physical properties
592 (Zonenshain and Le Pichon, 1986).

593 ***Early Miocene – Middle Miocene (Base of Sarmatian) (20.5-13 Ma)***

594 Exploration wells on the Crimean peninsula and offshore Romania recovered mudstones
595 in this interval (Robinson et al., 1995a; Spandini et al., 1996; Meredith and Egan, 2002; Nikishin
596 et al., 2003). Correlative units exposed onshore provide little information as they are fluvial,
597 evaporitic or volcanic, and are thus unlikely to be representative of their equivalents in the basin
598 center (Robinson et al., 1995a). Parallel reflections observed in seismic reflection sections imply
599 turbiditic sediments in this interval (Zonenshain and Le Pichon, 1986; Robinson et al., 1995a).

600 ***Middle Miocene (Base of Sarmatian) – Late Miocene (Top of Sarmatian) (13-11 Ma)***

601 This interval is thought to comprise terrigenous sediments, passively infilling the basin
602 center (Nikishin et al., 2003). Onshore exposures in Georgia are primarily sandy clastics (Banks
603 et al., 1997)

604 ***Late Miocene (Top of Sarmatian) – Top of Pliocene (11-1.8 Ma)***

Sands and conglomerates of Pliocene age have been drilled onshore Georgia (Chaladidi-13 and Chaladidi-14) and mapped in northeastern Turkey (Robinson et al., 1995b), though these units are typically non-marine and unlikely to be representative of lithologies in the basin center. Chalks, siderites, clays and limestone were recovered by DSDP drilling in the basin center (Ross, 1978; Hsü and Giovanoli, 1980). Interestingly, this interval also contains a thin unit comprising algal mats and peletal limestones, indicative of very shallow water depths (Ross, 1978; Hsü and Giovanoli, 1980; Kojumdgieva, 1983). Although interpretations regarding the age and causes of these deposits are controversial (Ross, 1978; Hsü and Giovanoli, 1980; Kojumdgieva, 1983), it appears that they correspond to a drop in sea level of over 2000 m, possibly related to Messinian desiccation event that affected the entire Mediterranean region (Hsü et al., 1973). Because this desiccation was likely short-lived (100 kyr) (Hsü and Giovanoli, 1980), it is not included in the subsidence analysis presented in this paper.

Top of Pliocene – Present (1.8-0 Ma)

The youngest sediments in the Black Sea have been recovered by gravity cores and drilling (Ross, 1978; Robinson et al., 1996; Aksu et al., 2002). Samples recovered at these locations consistently demonstrate that the uppermost sediments contain mostly clays, although they also include marls and occasional turbidites (Ross, 1978; Hsü and Giovanoli, 1980; Aksu et al., 2002; Hiscott and Aksu, 2002). Likewise, high-resolution seismic and sonar images also show primarily flat-lying, undisturbed sediments in the basin center, although the shallowest sediments do show occasional disruption by gas (Ergün et al., 2002).

625 **References**

626 Aksu, A. E., R. N. Hiscott, D. Yasar, F. I. Isler, and S. Marsh, 2002, Seismic stratigraphy of the
627 Late Quatenary deposits from the southwestern Black Sea shelf: evidence for non-
628 catastrophic variations in sea-level during the last ~10000 yr: Marine Geology, v. 190, p.
629 61-94.
630 Al-Lazki, A. I., E. Sandvol, D. Seber, M. Barazangi, N. Turkelli, and R. Mohamad, 2004, Pn
631 tomographic imaging of mantle lid velocity and anisotropy at the junction of the Arabian,
632 Eurasian and African plates: Geophys. J. Int., v. 158, p. 1024-1040.
633 Banks, C. J., A. G. Robinson, and M. P. Williams, 1997, Structure and regional tectonics of the
634 Achara-Trialet fold belt and the adjacent Rioni and Kartli foreland basins: AAPG
635 Memoir 68: Tulsa, OK, AAPG.
636 Bellingham, P., and N. White, 2002, A two-dimensional inverse model for extensional
637 sedimentary basins: 2. Application: J. Geophys. Res., v. 107, doi:10.1029/2001JB000174.
638 Belousov, V. V., B. S. Volvovsky, I. V. Arkhipov, V. B. Buryanova, Y. D. Evsyukov, V. P.
639 Goncharov, V. V. Gordienko, D. F. Ismagilov, G. K. Kislov, L. I. Kogan, V. N.
640 Moskalenko, Y. P. Neprchnov, B. K. Ostisty, O. M. Rusakov, K. M. Shimkus, A. E.
641 Shlenzinger, V. V. Sochelnikov, V. B. Sollogub, V. D. Solovyev, V. I. Starostenko, A. F.
642 Starovoitov, A. A. Terekhov, I. S. Volvovsky, A. S. Zhigunov, and V. G. Zolotarev,
643 1988, Structure and evolution of the earth's crust and upper mantle of the Black Sea:
644 Bollettino Di Geofisica Teorica ed Applicata, v. 30 p. 109-196.
645 Boztug, D., R. Jonckheere, G. A. Wagner, and Z. Yegingil, 2004, Slow Senonian and fast
646 Palaeocene-Early Eocene uplift of the granitoids in the Central Eastern Pontides, Turkey:
647 apatite fission-track results: Tectonophysics, v. 382, p. 213-228.
648 Bry, M., and N. White, 2007, Reappraising elastic thickness variation at oceanic trenches: J.
649 Geophys. Res., v. 112, doi:10.1029/2005JB004190.
650 Buck, W. R., F. Martinez, M. S. Steckler, and J. R. Cochran, 1988, Thermal Consequences of
651 Lithospheric Extension: Pure and Simple: Tectonics, v. 7, p. 213-234.
652 Burov, E. B., and M. Diament, 1995, The effective elastic thickness (*Te*) of continental
653 lithosphere: What does it really mean?: J. Geophys. Res., v. 100, p. 3905-3927.
654 Çakir, Ö., and M. Erduran, 2004, Constraining crustal and uppermost mantle structures beneath
655 station TBZ (Trabzon, Turkey) by receiver functions and dispersion analysis: Geophys. J.
656 Int., v. 158, p. 955-971.
657 Cloetingh, S., G. Spandini, J. D. Van Wees, and F. Beekman, 2003, Thermo-mechanical
658 modelling of the Black Sea Basin (de)formation: Sedimentary Geology, v. 156, p. 169-
659 184.
660 Davis, M., and N. Kusznir, 2004, Depth-Dependent Lithospheric Stretching at Rifted Continental
661 Margins, in G. D. Karner, J. D. Morris, N. W. Driscoll, and E. A. Silver, eds., Rheology
662 and Deformation of the Lithosphere: New York, NY, Columbia University Press, p. 92-
663 137.
664 Edwards, G. R. H., 2006, Inverse Modelling of Extensional Sedimentary Basins and Margins:
665 Doctoral thesis, University of Cambridge, Cambridge, 226 p.
666 Edwards, G. R. H., N. White, and J. Haines, in prep, Inverse modelling of extensional
667 sedimentary basins and margins: J. Geophys. Res.
668 Ergün, M., D. Dondurur, and G. Cifci, 2002, Acoustic evidence for shallow gas accumulations in
669 the sediments of the Eastern Black Sea: Terra Nova, v. 14, p. 313-320.

Finetti, I., G. Bricchi, A. Del Ben, M. Pipan, and Z. Xuan, 1988, Geophysical Study of the Black Sea: Bollettino Di Geofisica Teorica ed Applicata, v. XXX, p. 197-324.
Gök, R., E. Sandvol, N. Türkelli, D. Seber, and M. Barazangi, 2003, Sn attenuation in the Anatolian and Iranian plateau and surrounding regions: Geophys. Res. Lett., v. 30, 8042, doi:10.1029/2003GL018020.
Görür, N., 1988, Timing of opening of the Black Sea basin: Tectonophysics, v. 147, p. 247-262.
Görür, N., and O. Tüysüz, 1997, Petroleum Geology of the Southern Continental Margin of the Black Sea, in A. G. Robinson, ed., Regional and petroleum geology of the Black Sea and surrounding region: AAPG Memoir, v. 68: Tulsa, OK, AAPG, p. 241-254.
Gradstein, F. M., J. G. Ogg, A. G. Smith, and e. al., 2004, A Geologic Time Scale 2004: Cambridge, Cambridge University Press.
Hearn, T. M., and J. F. Ni, 1994, Pn velocities beneath continental collision zones: the Turkish-Iranian Plateau: Geophys. J. Int., v. 117, p. 273-283.
Hiscott, R. N., and A. E. Aksu, 2002, Late Quaternary history of the Marmara Sea and Black Sea from high-resolution seismic and gravity-core studies: Marine Geology, v. 190, p. 261-282.
Hopper, J. R., and W. R. Buck, 1998, Styles of extensional decoupling: Geology, v. 26, p. 699-702.
Hsü, K. J., and F. Giovanoli, 1980, Messian event in the Black Sea: Palaeogeography, Palaeoclimatology, Palaeoecology, v. 29, p. 75-83.
Hsü, K. J., W. B. F. Ryan, and M. B. Cita, 1973, Late Miocene desiccation of the Mediterranean: Nature, v. 242, p. 240-244.
IOC IHO BODC, 2003, Centenary Edition of the GEBCO Digital Atlas, published on CD-ROM on behalf of the Intergovernmental Oceaonographic Commission and the International Hydrographic Organization as part of the General Bathymetric Chart of the Oceans, Liverpool, British Oceanographic Data Centre.
Jones, R. W., and M. D. Simmons, 1997, A Review of the Stratigraphy of Eastern Paratethys (Oligocene-Holocene), With Particular Emphasis on th Black Sea, in A. G. Robinson, ed., Regional and petroleum geology of the Black Sea and surrounding region, v. 68, AAPG Memoir, p. 39-52.
Jones, S. M., N. White, P. Faulkner, and P. Bellingham, 2004, Animated models of extensional basins and passive margins: Geochem. Geophys. Geosyst., v. 5, Q08009, doi:10.1029/2003GC000658.
Kazmin, V. G., A. A. Schreider, and A. A. Bulychev, 2000, Early stages of evolution of the Black Sea, in E. Bozkurt, J. A. Winchester, and J. D. A. Piper, eds., Tectonics and Magmatism in Turkey and the Surrounding Area, v. Special Publications, 173: London, Geological Society, p. 235-249.
Kojumdgieva, E., 1983, Palaeogeographic Environment During the Desiccation of the Black Sea: Palaeogeography, Palaeoclimatology, Palaeoecology, v. 43, p. 195-204.
Kutas, R. I., V. P. Kobolev, and V. A. Tsvyashchenko, 1998, Heat flow and geothermal model of the Black Sea depression: Tectonophysics, v. 291, p. 91-100.
Lavier, L. L., and G. Manatschal, 2006, A mechanism to thin the continental lithosphere at magma-poor margins: Nature, v. 440, p. 324-328.
Letouzey, J., B. Biju-Duval, A. Dorkel, R. Gonnard, K. Kristchev, L. Montadert, and O. Sungurlu, 1977, The Black Sea: A Marginal Basin, Geophysical and Geological Data, in

715 B. Biju-Duval, and L. Montadert, eds., International Symposium of the Mediterranean
716 Basins Split (Yugoslavia) 25-29 October 1976: Paris, Editions Technip, p. 363-376.
717 McClusky, S., S. Balassanian, A. Barka, C. Demir, S. Ergintav, G. Georgiev, O. Gurkan, M.
718 Hamburger, K. Hurst, H. Kahle, K. Kastens, G. Kekelidze, R. King, V. Kotzev, O. Lenk,
719 S. Mahmoud, A. Mishin, M. Ndariya, A. Ouzounis, D. Paradissis, Y. Peter, M. Prilepin,
720 R. Reilinger, I. Sanli, H. Seeger, A. Tealeb, M. N. Toksöz, and G. Veis, 2000, Global
721 Positioning System constraints on plate kinematics and dynamics in the eastern
722 Mediterranean and Caucaus: J. Geophys. Res., v. 105, p. 5695-5719.
723 McKenzie, D., 1972, Active tectonics of the Mediterranean Region: Geophys. J. R. astr. Soc., v.
724 30, p. 109-185.
725 McKenzie, D., and D. Fairhead, 1997, Estimates of the effective elastic thickness of the
726 continental lithosphere from Bouguer and free air gravity anomalies: J. Geophys. Res., v.
727 102, p. 27,523-27,552.
728 McKenzie, D., F. Nimmo, J. A. Jackson, P. B. Gans, and E. L. Miller, 2000, Characteristics and
729 consequences of flow in the lower crust: J. Geophys. Res., v. 105, p. 11,029-11,046.
730 McKenzie, D. P., 1978, Some remarks on the development of sedimentary basins: Earth Planet.
731 Sci. Lett., v. 40, p. 25-32.
732 Meredith, D. J., and S. S. Egan, 2002, The geological and geodynamic evolution of the eastern
733 Black Sea basin: insights from 2-D and 3-D tectonic modelling: Tectonophysics, v. 350,
734 p. 157-179.
735 Minshull, T. A., N. J. White, R. A. Edwards, D. J. Shillington, C. L. Scott, A. Demirer, M.
736 Shaw-Champion, S. M. Jones, M. Erduran, T. Beselvi, G. Coskun, K. Raven, A. Price,
737 and B. Peterson, 2005, Seismic Data Reveal Eastern Black Sea Structure: Eos, v. 86, p.
738 413,416-7.
739 Nikishin, A. M., M. V. Korotaev, A. V. Ershov, and M.-F. Brunet, 2003, The Black Sea basin:
740 tectonic history and Neogene-Quaternary rapid subsidence modelling: Sedimentary
741 Geology, v. 156, p. 149-168.
742 Okay, A. I., A. M. C. Sengor, and N. Görür, 1994, Kinematic history of the opening of the Black
743 Sea and its effect on the surrounding regions: Geology, v. 22, p. 267-270.
744 Parsons, B., and J. G. Sclater, 1977, An Analysis of the Variation in Ocean Floor Bathymetry
745 and Heat Flow with Age: J. Geophys. Res., v. 82, p. 803-827.
746 Perez-Gussinye, M., A. R. Lowry, A. B. Watts, and I. Velicogna, 2004, On the recovery of
747 effective elastic thickness using spectral methods: Examples from synthetic data and
748 from the Fennoscandia Shield: J. Geophys. Res., v. 109, doi: 10.1029/2003JB002788.
749 Press, W. H., S. A. Teukolsky, W. T. Vetterling, and B. P. Flannery, 1992, Numerical Recipes in
750 Fortran 77: the art of scientific computing: Cambridge, Cambridge University Press.
751 Rangin, C., A. G. Bader, G. Pascal, B. Ecevitoglu, and N. Görür, 2002, Deep structure of the
752 Mid Black Sea High (offshore Turkey) imaged by multi-channel seismic survey
753 (BLACKSIS cruise): Marine Geology, v. 182, p. 265-278.
754 Reilinger, R., S. McClusky, P. Vernant, S. Lawrence, S. Ergintav, R. Cakmak, H. Ozener, F.
755 Kadirov, I. Guliev, R. Stepanyan, M. Nadariya, G. Hahubia, S. Mahmoud, K. Sakr, A.
756 ArRajehi, D. Paradissis, A. Al-Aydrus, M. Prilepin, T. Guseva, E. Evren, A. Dmitrotsa,
757 S. V. Filikov, F. Gomez, R. Al-Ghazzi, and G. Karam, 2006, GPS constraints on
758 continental deformation in the Africa-Arabia-Eurasia continental collision zone and
759 implications for the dynamics of plate interactions: J. Geophys. Res., v. 111,
760 doi:10.1029/2005JB004051.

761 Robertson, A. H. F., T. Ustaömer, E. A. Pickett, A. S. Collins, T. Andrew, and J. E. Dixon, 2004,
762 Testing models of Late-Palaeozoic-Early Mesozoic orogeny in Western Turkey: support
763 for an evolving open-Tethys model: J. Geol. Soc. London, v. 161, p. 501-511.
764 Robinson, A., G. Spandini, S. Cloetingh, and J. Rudat, 1995a, Stratigraphic Evolution of the
765 Black Sea: inferences from basin modelling: Marine Pet. Geol., v. 12, p. 831-835.
766 Robinson, A. G., C. J. Banks, M. M. Rutherford, and J. P. P. Hirst, 1995b, Stratigraphic and
767 structural development of the Eastern Pontides, Turkey: J. Geol. Soc. London, v. 152, p.
768 861-872.
769 Robinson, A. G., J. H. Rudat, C. J. Banks, and R. L. F. Wiles, 1996, Petroleum Geology of the
770 Black Sea: Marine Petrol. Geol., v. 13, p. 195-223.
771 Ross, D. A., 1978, Summary of results of Black Sea drilling, Init. Rep. DSDP, v. 42, p. 1149-
772 1177.
773 Ross, D. A., Y. P. Neprchnov, K. J. Hsu, E. S. Trimonis, S. F. Percival, Jr., A. J. Erickson, E. T.
774 Degens, J. M. Hunt, F. T. Manheim, M. Senalp, A. Traverse, and P. Stoffers, 1978, Leg
775 42, Part 2, of the cruises of the drilling vessel Glomar Challenger; Istanbul, Turkey to
776 Istanbul, Turkey, May-June 1975, DSDP.
777 Rudat, J. H., and D. S. Macgregor, 1993, Unconventional exploration techniques in a high cost
778 deep water basin: a case study from the Black Sea: Soc. of Explor. Geophys. Abstr.
779 Progr.
780 Saintot, A., and J. Angelier, 2002, Tectonic paleostress fields and structural evolution of the
781 NW-Caucaus fold-and-thrust belt from Late Cretaceous to Quaternary: Tectonophysics,
782 v. 357, p. 1-31.
783 Sclater, J. G., and P. A. F. Christie, 1980, Continental Stretching: An Explanation of the Post-
784 Mid-Cretaceous Subsidence of the Central North Sea Basin: J. Geophys. Res., v. 85, p.
785 3711-3739.
786 Spandini, G., A. Robinson, and S. Cloetingh, 1996, Western versus Eastern Black Sea tectonic
787 evolution: pre-rift lithospheric controls on basin formation: Tectonophysics, v. 266, p.
788 139-154.
789 Spandini, G., A. G. Robinson, and S. A. P. L. Cloetingh, 1997, Thermomechanical Modeling of
790 Black Sea Basin Formation, Subsidence and Sedimentation, in A. G. Robinson, ed.,
791 Regional and petroleum geology of the Black Sea and surrounding region, v. 68: Tulsa,
792 AAPG Memoir, p. 19-38.
793 Starostenko, V., V. Buryanov, I. Makarenko, O. Rusakov, R. Stephenson, A. Nikishin, G.
794 Georgiev, M. Gerasimov, R. Dimitriu, O. Legostaeva, V. Pchelarov, and C. Sava, 2004,
795 Topography of the crust-mantle boundary beneath the Black Sea Basin: Tectonophysics,
796 v. 381, p. 211-233.
797 Steckler, M. S., and A. B. Watts, 1978, Subsidence of the Atlantic-type Continental Margin off
798 New York: Earth Planet. Sci. Lett., v. 41, p. 1-13.
799 Turcotte, D. L., and G. Schubert, 2002, Geodynamics: Cambridge, UK, Cambridge University
800 Press.
801 Ustaömer, T., and A. H. F. Robertson, 1997, Tectonic-Sedimentary Evolution of the North
802 Tethyan Margin in the Central Pontides of Northern Turkey, in A. G. Robinson, ed.,
803 Regional and petroleum geology of the Black Sea and surrounding regions: AAPG
804 Memoir 68: Tulsa, OK, AAPG, p. 255-290.

805 Vincent, S. J., M. B. Allen, A. D. Ismail-Zadeh, R. Flecker, K. A. Foland, and M. D. Simmons,
806 2005, Insights from the Talysh of Azerbaijan into the Paleogene evolution of the South
807 Caspian region: GSA Bulletin, v. 117, p. 1513-1533.
808 Wernicke, B., 1985, Uniform-sense of normal sense simple-shear of the continental lithosphere:
809 Can. J. Earth Sci., v. 22, p. 108-125.
810 White, N., 1993, Recovery of strain rate variation from inversion of subsidence data: Nature, v.
811 366, p. 449-452.
812 White, N., and P. Bellingham, 2002, A two-dimensional inverse model for extensional
813 sedimentary basins: 1. Theory: J. Geophys. Res., v. 107, p. doi: 10.1029/2001JB000173.
814 Whitmarsh, R. B., G. Manatschal, and T. A. Minshull, 2001, Evolution of magma-poor
815 continental margins from rifting to seafloor spreading: Nature, v. 413, p. 150-153.
816 Yilmaz, Y., O. Tüysüz, E. Yigitbas, S. Genç, Can, and A. M. C. Sengör, 1997, Geology and
817 Tectonic Evolution of the Pontides, in A. G. Robinson, ed., Regional and petroleum
818 geology of the Black Sea and surrounding region: AAPG Memoir 68: Tulsa, AAPG, p.
819 183-226.
820 Zonenshain, L. P., and X. Le Pichon, 1986, Deep Basins of the Black Sea and Caspian Sea as
821 Remnants of Mesozoic Back-Arc Basins: Tectonophysics, v. 123, p. 181-211.
822 Zor, E., E. Sandvol, C. Gürbüz, N. Türkelli, D. Seber, and M. Barazangi, 2003, The crustal
823 structure of the East Anatolian plateau (Turkey) from receiver functions: Geophys. Res.
824 Lett., v. 30, p. 8044.
825
826

827 **Figure Captions**

828

829 Figure 1. Map of the eastern Black Sea showing Cenozoic sediment thickness in the center of
830 the basin and illuminated elevation from GEBCO (IOC IHO BODC, 2003) outside the basin.
831 Sediment thickness is estimated from seismic reflection profiles. The transect used for
832 subsidence analysis is indicated with a black line. Other major features are also labeled and
833 discussed further in Sections 2-4. White circles indicate earthquakes with magnitudes >3 that
834 occurred from Aug. 2005 - Aug. 2006 and are scaled by magnitude; these were taken from the
835 online catalogue of the Centre Sismologique Euro-Méditerranéen. The inset in the upper right
836 hand corner gives the location of the study area with respect to the entire Black Sea and shows
837 the locations of academic and industry wells around the Black Sea that are discussed in the text.

838

839 Figure 2. a. Seismic reflection profiles KDZ 91-43 and 8040 (Robinson et al., 1996), which
840 correspond with the subsidence analysis along the profile whose location is shown in Fig. 1. The
841 inset shows the depth-time relationship derived from stacking velocities, which was used to
842 convert seismic stratigraphic horizons to depth. The black line indicates depth-time function in
843 the center of the basin averaged over 150 km, and grey shading indicates +/- one standard
844 deviation. b. Interpreted section showing the horizons and ages used for subsidence analysis and
845 other major features observed on these lines.

846

847 Figure 3. Stratigraphic column from the center of the eastern Black Sea estimated from onshore
848 geologic mapping, existing well control and seismic reflection data, which are described in the
849 Appendix. Three different cases of paleowater depth (PWD) variations are shown in the third to

850 fifth columns; each of these is modeled during strain rate inversion to address uncertainties in
851 this parameter. In each case, the depth shown is the depth in the deepest part of the basin. The
852 sixth column shows the PWD estimates/assumptions employed in previous studies (Robinson et
853 al., 1995a; Meredith and Egan, 2002; Cloetingh et al., 2003; Nikishin et al., 2003). Note that our
854 three PWD cases encompass many of the variations inferred or estimated by previous studies.
855 Estimated ages for each horizon are taken from previous work. Tectonic events in the right
856 column are taken from Boztug et al. (Boztug et al., 2004) and Saintot et al. (Saintot and Angelier,
857 2002).
858
859 Figure 4. Results from both depth-uniform (left column) and depth-dependent strain rate
860 inversion (middle and right columns) for the PWD Case 1 assuming Airy isostasy. Illustrated in
861 Figure 3 and described in Section 7.1. The upper panels show the match between flexurally
862 backstripped stratigraphic horizons that served as input (black lines) and model predictions (red
863 dashed lines). For the depth-uniform model, the middle panel is a grid showing spatial and
864 temporal variations in strain rate. The lower panel shows cumulative beta at each time step
865 (black lines) and beta calculated from preliminary velocity model from wide-angle seismic
866 refraction data (dashed grey line) (Minshull et al., 2005). The four panels in the middle and right
867 columns are orthogonal slices through strain rate cube produced by depth-dependent inversion.
868 The panels in the middle column are depth slices at 0 km depth (which can be compared with
869 depth-uniform result) and 120 km depth. The right panels are time slices at 58.5 Ma and 13 Ma.
870

871 Figure 5. Results from both depth-uniform (left column) and depth-dependent strain rate
872 inversion (middle and right columns) for the PWD Case 2 assuming Airy isostasy. Illustrated in
873 Figure 3 and described in Section 7.2. See Figure 4 caption for explanation of panels.
874
875 Figure 6. Results from both depth-uniform (left column) and depth-dependent strain rate
876 inversion (middle and right columns) for the PWD Case 3 assuming Airy isostasy. Illustrated in
877 Figure 3 and described in Section 7.3. See Figure 4 caption for explanation of panels.
878
879 Figure 7. a. Results of pure-shear strain rate inversion using PWD Case 1 and different values for
880 T_e (0, 20, 50, 100 km). Notice that larger strain rates and stretching factors are recovered by
881 inversion when larger values for T_e are used. b. Results of strain rate inversion using PWD Case
882 2 and different values for T_e. c. Misfit as a function of T_e for PWD Cases 1 and 2. d. Match
883 between predicted curvature of Shatsky Ridge for various values of T_e based on a pointed-loaded
884 broken elastic beam (dotted blue lines) and average of curvature of Shatsky Ridge over 40 km
885 along strike (black line). Grey shaded area indicates ±1 standard deviation of averaged profiles
886 and serves as the uncertainty for T_e estimation. Inset shows misfit function; a T_e of 2.3 km best
887 fits the data, and values of T_e between 2-3 km fit data with a chi-squared of <1.
888
889 Figure 8. Possible examples of growth in reflection data from a. Sinop trough, line KDZ 91-43a;
890 b. center of the EBS, line 8037.
891
892 Figure 9. β variations over entire eastern Black sea estimated from the relationship between
893 sediment thickness and β for PWD Case 1. The large map shows contoured estimated β over the

EBS following spatial filtering of 40 km. Dark shading indicates high β values. The maximum estimated β in the basin is ~5-6. Regions with poor data coverage or that are strongly affected by compression (e.g., around Tuapse trough) have been masked. The inset shows the relationship between β and sediment thickness based on subsidence analyses presented in Figure 4. The black line represents the best fitting polynominal, which was used to estimate β across the basin. The grey band indicates ±1 standard deviation.

Suppl. Figure Captions

Suppl. Figure 1. a. Input horizons along the profile following depth conversion. b. Input horizons following backstripping assuming PWD for Case 1, where shallow PWD was associated with the end of the Cretaceous (0—200 km), and deep PWD was present afterwards (2000—2200 m). Colored lines indicated results of backstripping using different values for T_e (0, 20, 50, 100 km). c. Input horizons following backstripping assuming PWD for Case 2, where deep PWD characterized the basin from the end of Cretaceous to the present. d. Input horizons following backstripping assuming PWD for Case 3, where shallow PWD was associated with the basin until the end of Pliocene times (0-200 m), and deep PWD was present afterwards.

Table 1, Shillington et al.

PWD Case	*Max. strain rate 65-45 Ma (m.y.$^{-1}$)*	*Max. strain rate 65-45 Ma (s^{-1})*	*Max strain rate 20-0 Ma (m.y.$^{-1}$)*	*Max strain rate 20-0 Ma (s^{-1})*	*Chi-squared*
Case 1, depth-uniform	0.0798	2.53×10^{-15}	0.0231	7.33×10^{-16}	2.089
Case 1, depth-dependent	0.0847	2.68×10^{-15}	0.0265	8.40×10^{-16}	0.860
Case 2, depth-uniform	0.0147	4.66×10^{-16}	0.0301	9.55×10^{-16}	2.324
Case 2, depth-dependent	0.0189	5.99×10^{-16}	0.0246	7.81×10^{-16}	0.859
Case 3, depth-uniform	0.0433	1.37×10^{-15}	0.1781	5.65×10^{-15}	6.379
Case 3, depth-dependent	0.0423	1.34×10^{-15}	0.1868	5.92×10^{-15}	3.007

Figure 1, Shillington et al.

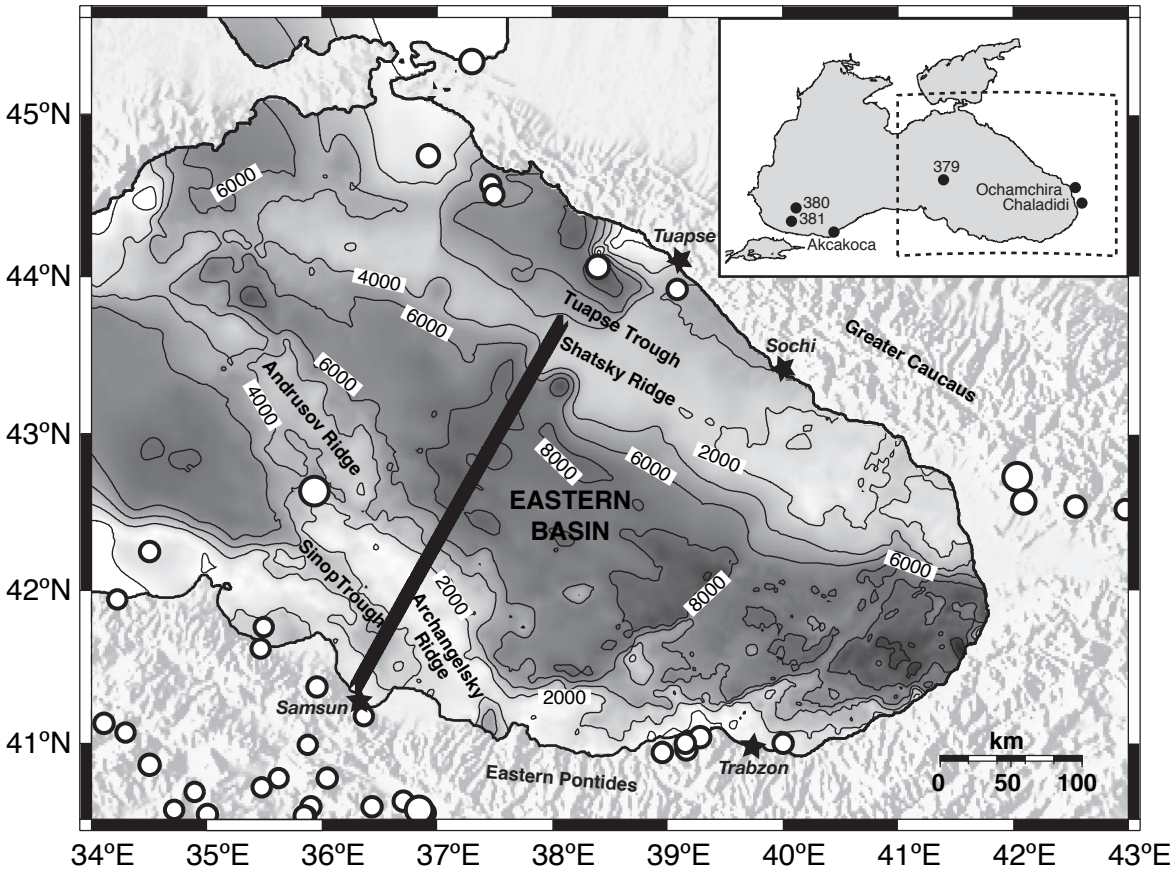

Figure 2, Shillington et al.

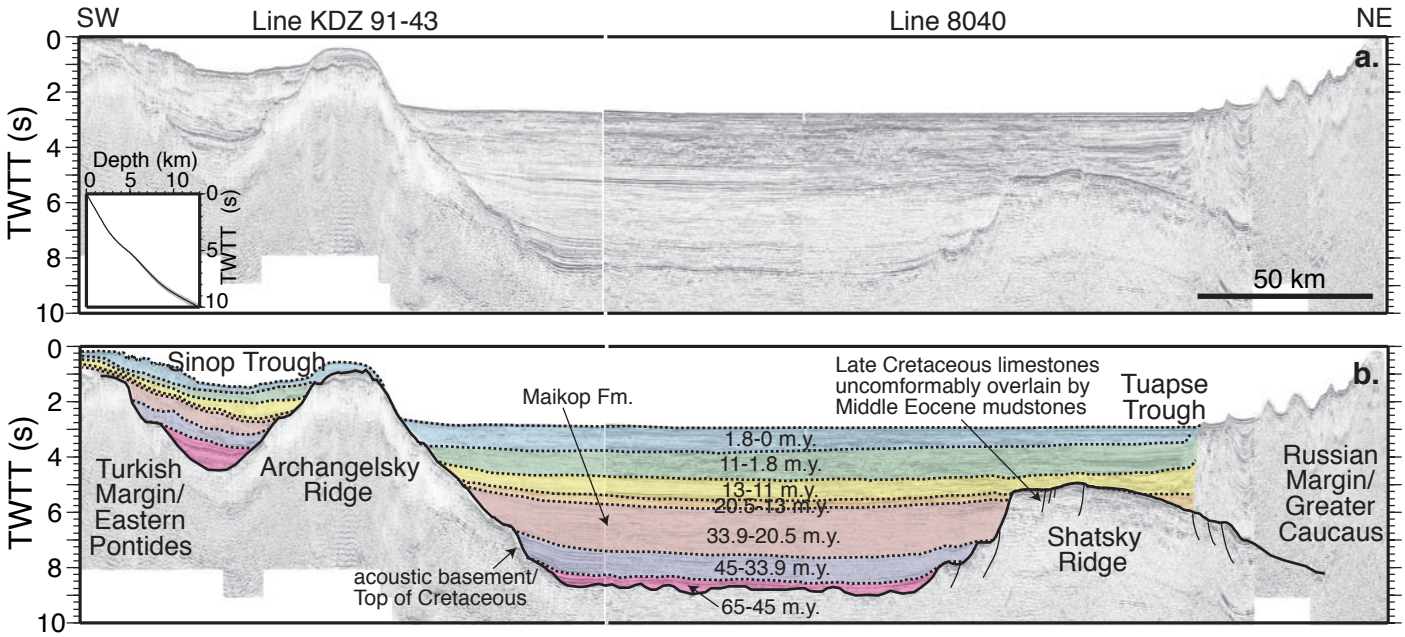

Figure 3, Shillington et al.

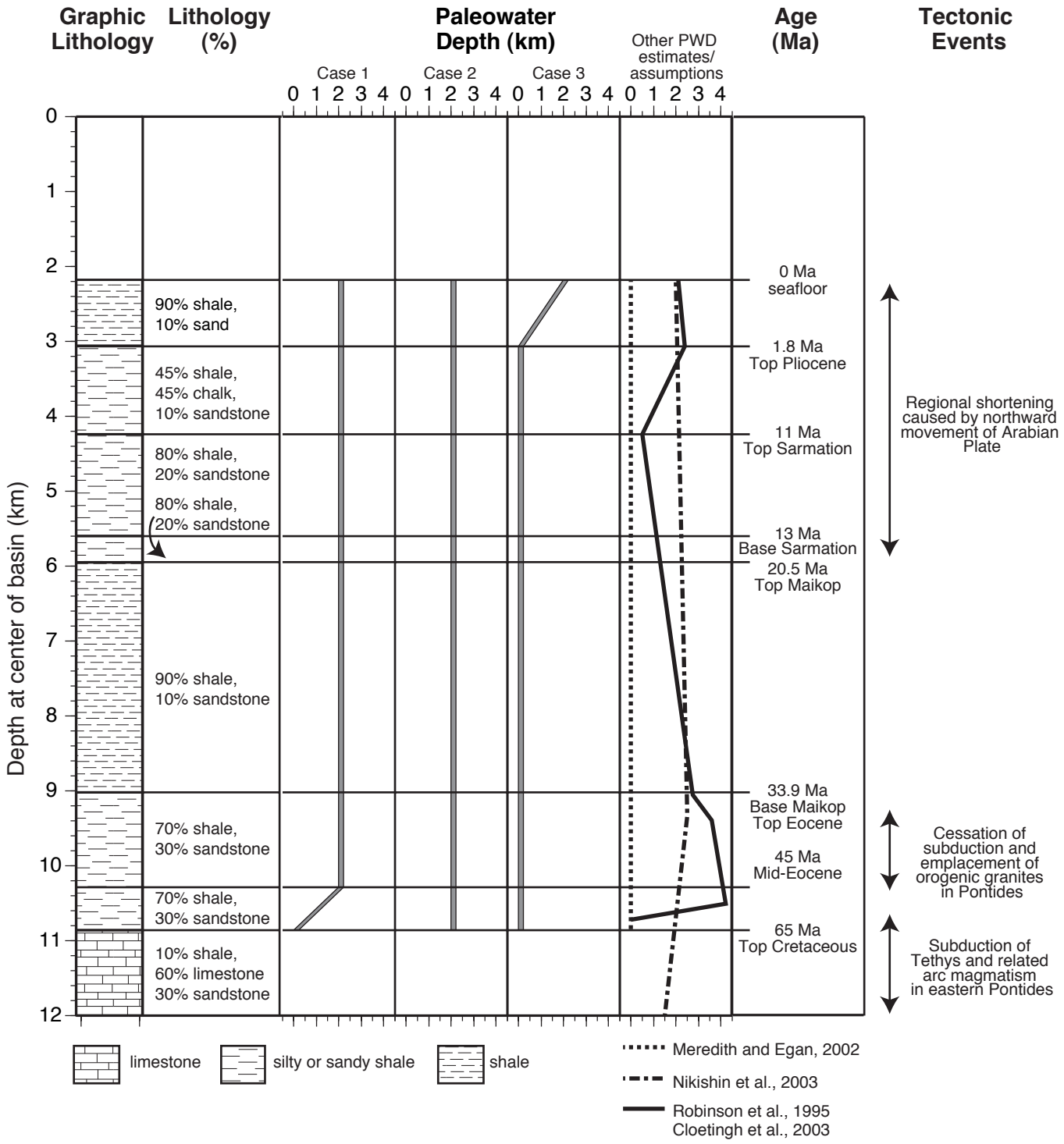

Figure 4, Shillington et al.

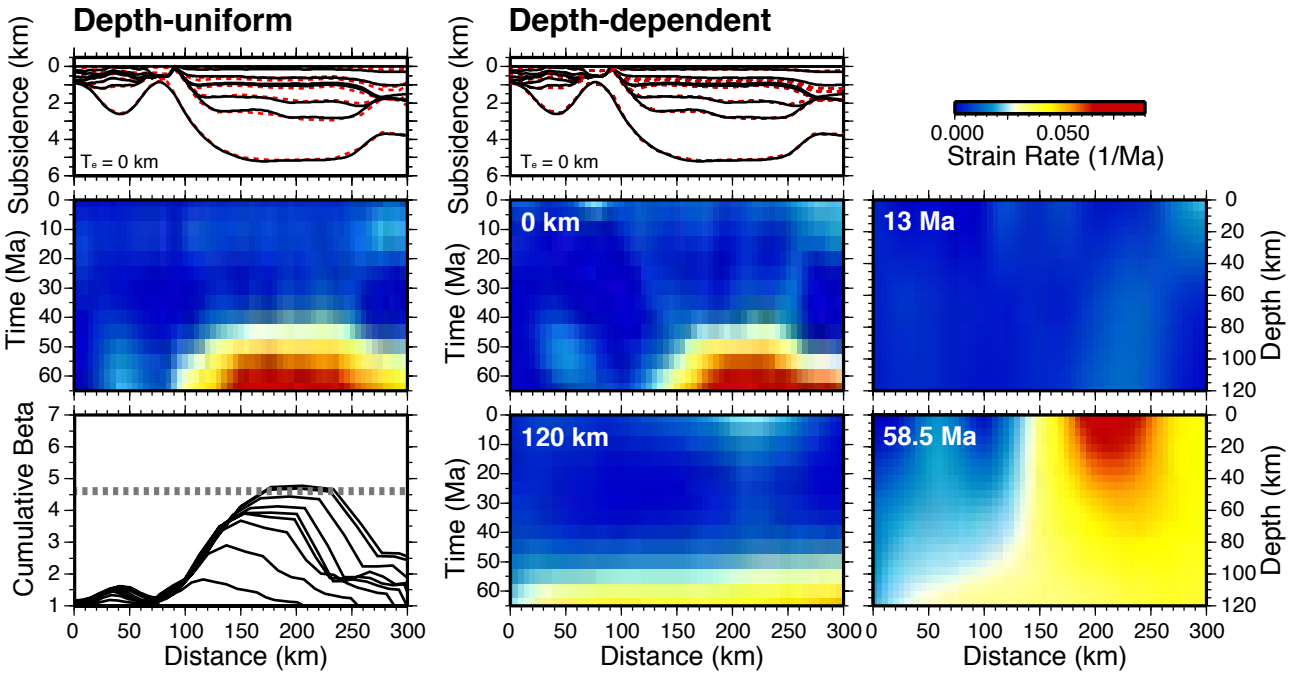

Figure 5, Shillington et al.

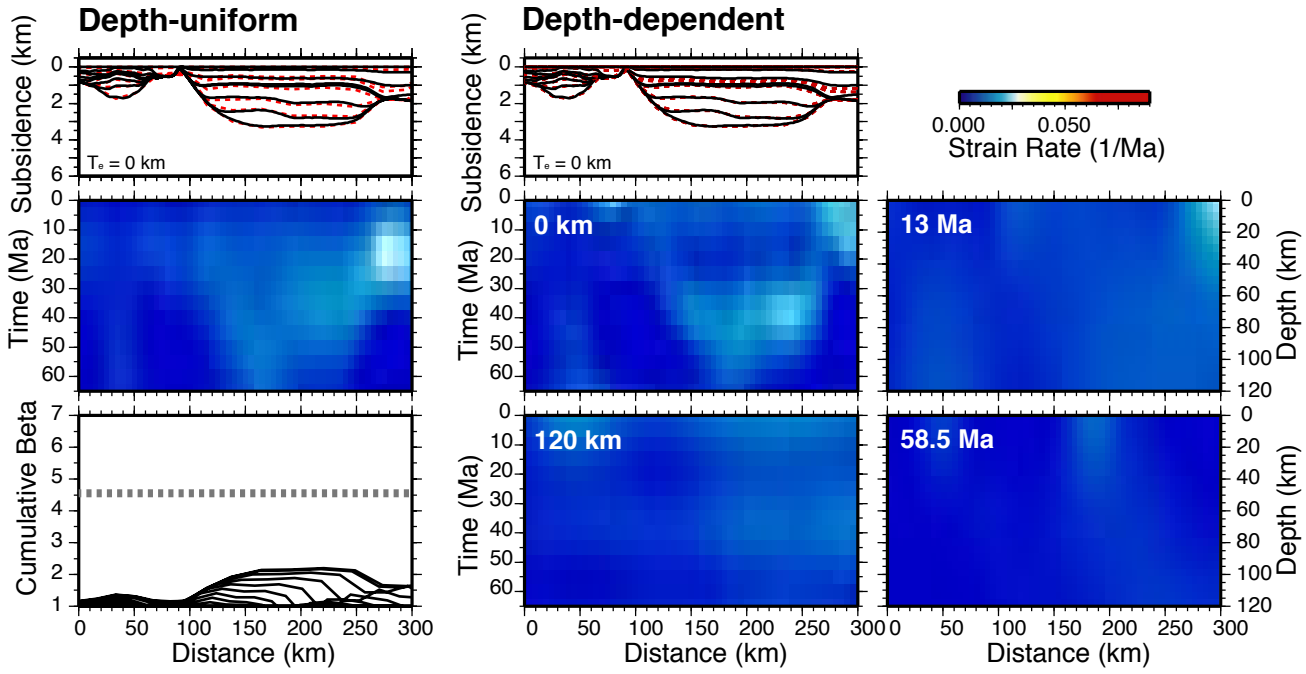

Figure 6, Shillington et al.

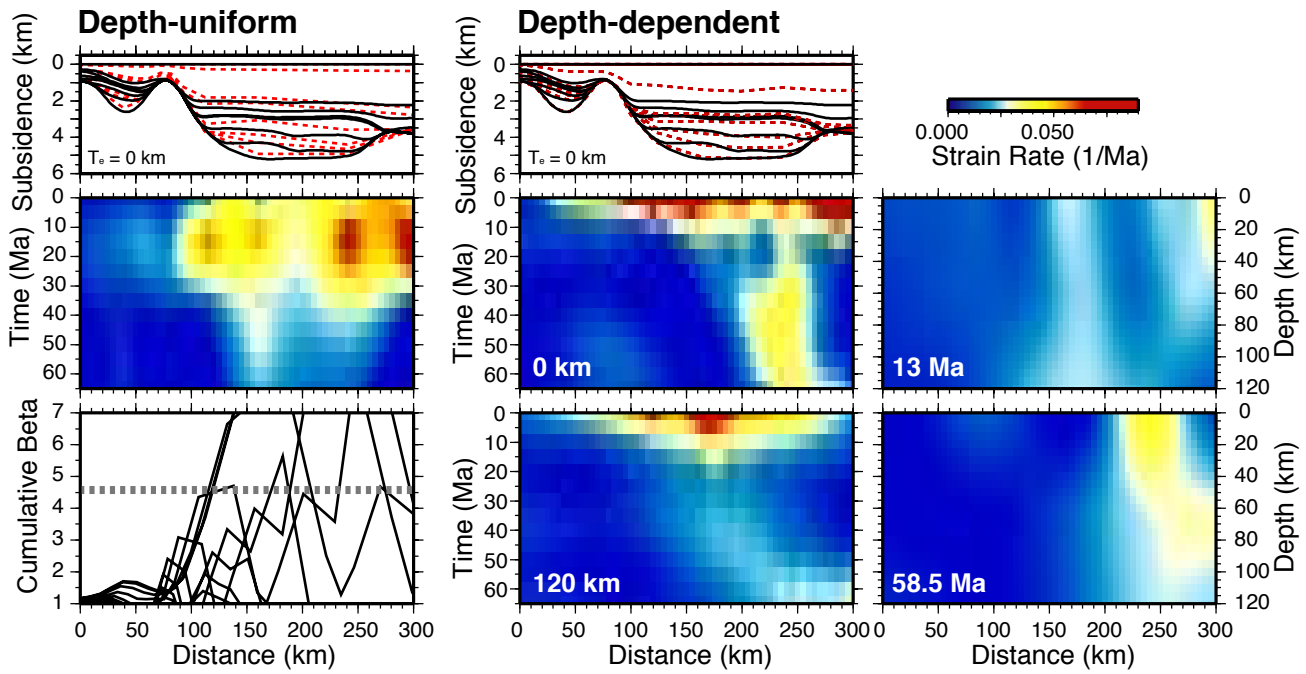

Figure 7, Shillington et al.

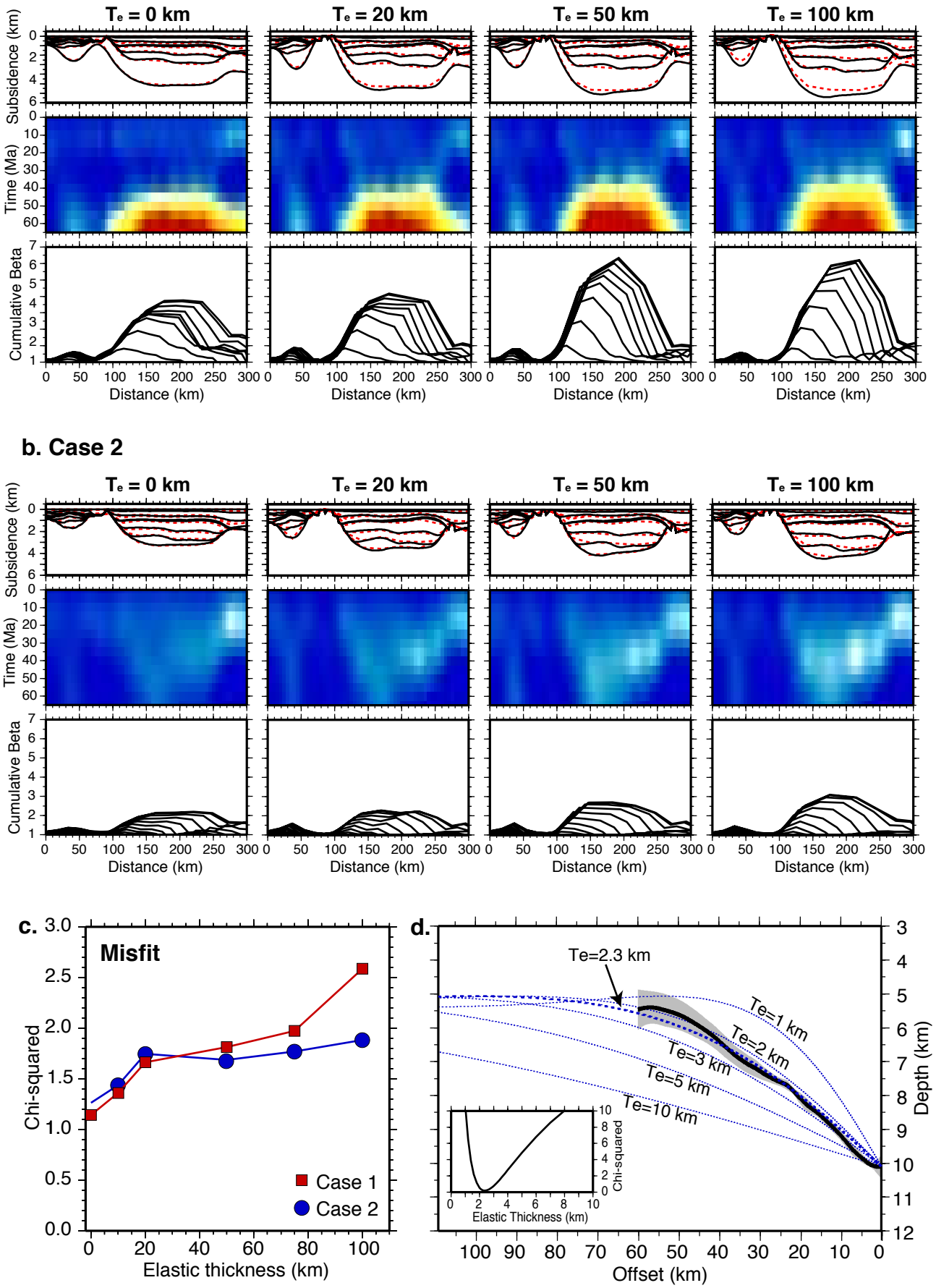

Figure 8, Shillington et al.

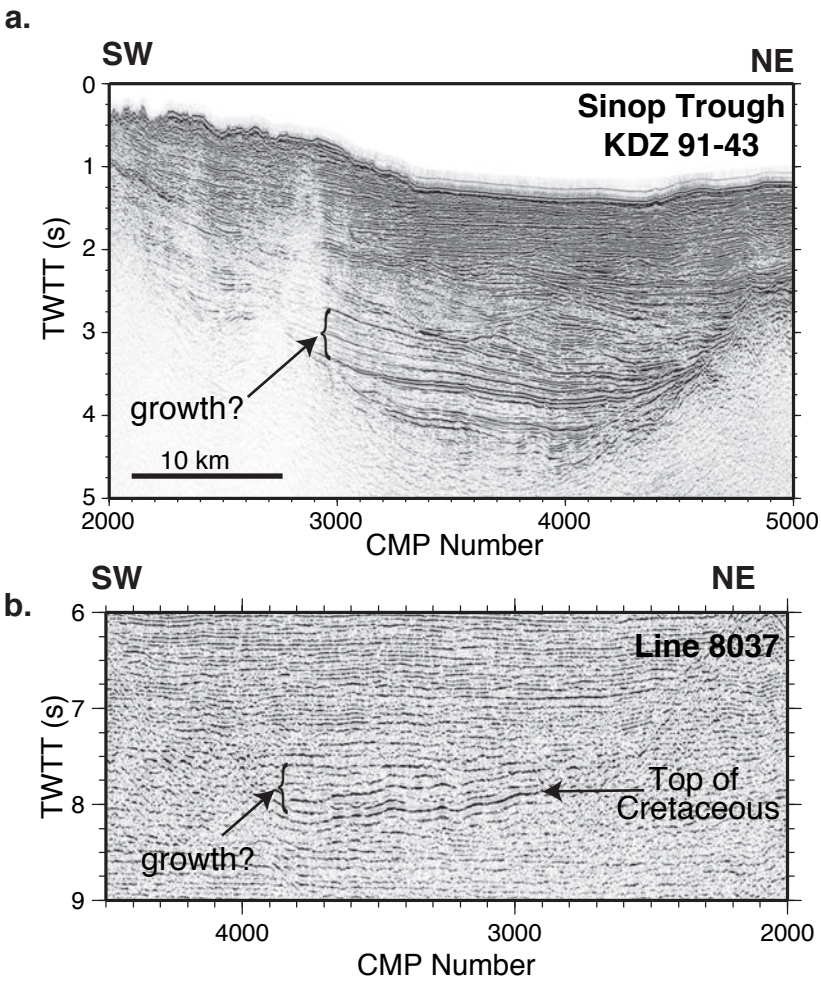

Figure 9, Shillington et al.